PHYSICS OF FLUIDS **26**, 027105 (2014)

Wave–vortex interactions in the nonlinear Schrödinger equation

Yuan Guo[a] and Oliver Bühler
Courant Institute of Mathematical Sciences, New York University, New York, New York 10012, USA

(Received 13 October 2013; accepted 3 February 2014; published online 21 February 2014)

This is a theoretical study of wave–vortex interaction effects in the two-dimensional nonlinear Schrödinger equation, which is a useful conceptual model for the limiting dynamics of superfluid quantum condensates at zero temperature. The particular wave–vortex interaction effects are associated with the scattering and refraction of small-scale linear waves by the straining flows induced by quantized point vortices and, crucially, with the concomitant nonlinear back-reaction, the remote recoil, that these scattered waves exert on the vortices. Our detailed model is a narrow, slowly varying wavetrain of small-amplitude waves refracted by one or two vortices. Weak interactions are studied using a suitable perturbation method in which the nonlinear recoil force on the vortex then arises at second order in wave amplitude, and is computed in terms of a Magnus-type force expression for both finite and infinite wavetrains. In the case of an infinite wavetrain, an explicit asymptotic formula for the scattering angle is also derived and cross-checked against numerical ray tracing. Finally, under suitable conditions a wavetrain can be so strongly refracted that it collapses all the way onto a zero-size point vortex. This is a strong wave–vortex interaction by definition. The conditions for such a collapse are derived and the validity of ray tracing theory during the singular collapse is investigated. [http://dx.doi.org/10.1063/1.4865837]

I. INTRODUCTION

Wave–vortex interactions are a classical topic in fluid dynamics, with well-known applications including vortices created by dissipating sound waves as in acoustic streaming and the so-called "quartz wind,"[1] longshore currents and rip currents created by breaking surface waves on beaches,[2] or the micro-mixing of fluid droplets based on stirring by waves.[3] Arguably, the field in which the relevant interaction theory is most advanced is that of atmosphere ocean fluid dynamics, because there it is well recognized that the nonlinear interactions between unresolved small-scale waves and the resolved large-scale mean flow are crucial for the long-term dynamics of the system, and therefore are crucial to climate prediction. This has led to a very detailed study of many wave–mean interaction effects in this field, accounts of which can now be found in standard textbooks and research monographs.[4–6]

Another physical scenario in which wave–vortex interactions are well known to be clearly important is the quantum superfluid dynamics of dilute Bose–Einstein condensates, in which there are lively interactions between various forms of dispersive waves and the peculiar quantum line vortices that allow the superfluid fluid component to perform a kind of vortex dynamics that in many ways is closely analogous to that of classical line vortices in incompressible fluid dynamics.[7–9] Of course, a detailed description of quantum superfluid dynamics at finite temperature is a complicated field-theoretic affair, which goes significantly beyond fluid dynamics.[10] Still, going back to the pioneering work of Landau,[26] there are practically useful two-fluid models, in which an intimate mixture of

[a]Email: yuanguo@cims.nyu.edu

a "normal" and a "super" fluid component joined together through various coupling mechanisms is considered. However, the complexity of these two-fluid models[11,12] makes it somewhat hard to extract fundamental fluid-dynamical information from them, especially as the coupling mechanism in them are themselves models for more microscopic, fundamental wave–vortex interactions.

A special conceptual place is therefore reserved for the very simple but powerful superfluid models based on the (defocusing) nonlinear Schrödinger equation (NLS), also known as the Gross–Pitaevskii equation in this field.[13,14] Whatever the context, the NLS equation has a well-known fluid-dynamical interpretation via the Madelung transformation, which allows comparing and contrasting classical and quantum fluid dynamics on an even footing.[15] Strictly speaking, the NLS equation can only model the Bose–Einstein condensate, which is closely related to superfluid behaviour[16] at zero temperature, but as a model for this limiting case it is of striking simplicity. Moreover, the NLS equation appears as a model equation in many other fields, ranging from nonlinear fibre optics to modulated surface waves, so fundamental studies of its intrinsic dynamical behaviour are valuable in its own right. This motivated the present study.

The particular wave–vortex interactions considered here are two-dimensional problems in which a slowly varying wavetrain of linear waves is scattered due to refraction by the straining flow induced by point vortices, which are located at a large distance from the wavetrain. In particular, we compute both the scattering of the linear waves as well as the concomitant nonlinear back-reaction onto the vortices that arises at second order in wave amplitude, and which manifests itself as a certain sideways advection of the vortex by a wave-induced mean flow. This builds on an earlier study in two-dimensional classical compressible fluid dynamics reported in Bühler and McIntyre[17](hereafter referred to as BM03),[17] in which this novel interaction effect was called the *remote recoil*. The present setting with the NLS equation differs in several important aspects from this earlier study, in which the wave dynamics was restricted to non-dispersive acoustic waves and in which the vortices in question were compactly supported, but finite-sized patches of vorticity. In contrast, in the NLS equation the waves are strongly dispersive and the vortices are necessarily point vortices of zero size. This necessitates a significant adjustment of the tools required to study this process.

Our main theoretical result is a description of the detailed wavenumber-dependence of the wave scattering process as well as of the concomitant recoil felt by the point vortices. Moreover, there is a novel possibility of extremely strong wave refraction by the point vortex that leads to a singular collapse of the wavetrain all the way into the location of the point vortex. The possibility of such a wavetrain collapse in classical acoustic problem had been noted long ago,[18] but only in the NLS equation can the collapse proceed all the way to the zero-size vortex line. We investigate approximately the linear wave dynamics of this fascinating wave collapse case in the NLS equation, but we were not able to compute the nonlinear wave–vortex interaction in this singular case. Some speculations as to what these interactions might be based on experience with classical fluid dynamics are offered in Sec. VII.

The paper is organized as follows. In Sec. II, governing equations are derived and the standard ray-tracing theory is summarized. Sec. III gives the setup for a finite wavetrain scattered by a single vortex and Sec. IV extends this to the scattering of infinite wavetrains. Theoretical results are derived and cross-checked by numerical integration of ray-tracing equations. Sec. V then expands the results to situations with multiple vortices. Sec. VI contains a study of rays being trapped by a vortex and Sec. VII offers concluding remarks.

II. GOVERNING EQUATIONS AND LINEAR WAVES

A. Nonlinear Schrödinger equation

The (defocusing) NLS, also called the Gross–Pitaevskii equation, is a well-known idealized model for the dynamics of a quantum system of weakly interacting identical bosons near absolute zero temperature, such as dilute Bose–Einstein condensates,[9,13] which are often realized experimentally using alkali gases.

The equation governs the complex-valued wave function ψ defined such that $|\psi|^2$ is the number density of the particles. Our detailed analysis will be in two space dimensions, but the general

equations hold in any number of spatial dimensions. In dimensional form, the NLS is

$$i\hbar\frac{\partial\psi}{\partial t} = -\frac{\hbar^2}{2m}\nabla^2\psi + [U_0|\psi|^2 + V]\psi, \tag{1}$$

where $\hbar$ is Planck's constant divided by 2π, U_0 is a positive constant modeling particle repulsion, m is the mass of a particle, and $V(\boldsymbol{x}, t)$ is an external potential, which we choose as $V = -U_0 n_0(1+\varphi)$ with n_0 being the density $|\psi|^2$ at infinity and φ being a forcing potential discussed later. The dimensional healing or coherence length[9] is defined by

$$\xi = \frac{\hbar}{\sqrt{mn_0U_0}}. \tag{2}$$

It is the characteristic length over which the density relaxes from zero at solid walls or vortex locations to its background value n_0.

All the dimensional parameters can be eliminated by using non-dimensional variables. For example, denoting non-dimensional variables with a prime we may choose

$$x = \frac{\hbar}{\sqrt{mn_0U_0}}x' = \xi x', \quad t = \frac{\hbar}{n_0U_0}t', \quad \text{and} \quad \psi = \sqrt{n_0}\psi'. \tag{3}$$

Dropping the primes, the non-dimensional NLS equation is

$$i\frac{\partial\psi}{\partial t} = -\frac{1}{2}\nabla^2\psi + (|\psi|^2 - 1)\psi - \psi\varphi. \tag{4}$$

If $\varphi = 0$, then the following integrals for mass, momentum, and energy are conserved:

$$N = \int |\psi|^2 d\boldsymbol{x}, \quad \boldsymbol{P} = \int \mathrm{Im}(\psi^*\nabla\psi)d\boldsymbol{x}, \tag{5}$$

$$\text{and} \quad \mathcal{E} = \int \left\{\frac{1}{2}|\nabla\psi|^2 + \frac{1}{2}(|\psi|^2 - 1)^2\right\} d\boldsymbol{x}. \tag{6}$$

Here, * denotes complex conjugation. If $\varphi \neq 0$, then the mass is still conserved, but the momentum and energy may change as described in (14) below.

B. Madelung transformation

The well-known Madelung transformation[19] allows a fluid-dynamical interpretation of the NLS equation, but the physical nature of the "fluid" of course depends on the specific application at hand. In the present context, there is an actual fluid present, namely, the dilute Bose–Einstein condensate, so here the interpretation is straightforward. The transform is based on the polar representation

$$\psi = \sqrt{h}\exp(i\theta), \tag{7}$$

where $h(\boldsymbol{x}, t) \geq 0$ and $\theta(\boldsymbol{x}, t)$ are real-valued functions describing the particle density and the phase of the wave function, respectively. In terms of $h = |\psi|^2$ and the velocity vector

$$\boldsymbol{u} = \nabla\theta = \frac{\mathrm{Im}(\psi^*\nabla\psi)}{|\psi|^2}, \tag{8}$$

the three integrals in (6) become

$$N = \int h\, d\boldsymbol{x}, \quad \boldsymbol{P} = \int h\boldsymbol{u}\, d\boldsymbol{x},$$
$$\text{and} \quad \mathcal{E} = \int \left(\frac{h}{2}|\boldsymbol{u}|^2 + \frac{|\nabla h|^2}{8h} + \frac{(h-1)^2}{2}\right) d\boldsymbol{x}. \tag{9}$$

Substituting (7) into (4) and separating real and imaginary parts yields

$$\frac{\partial h}{\partial t} + \nabla \cdot (h\boldsymbol{u}) = 0 \qquad \text{(continuity equation)}, \tag{10}$$

$$\frac{\partial \theta}{\partial t} + \frac{|\boldsymbol{u}|^2}{2} + (h-1) - \varphi = \frac{\nabla^2\sqrt{h}}{2\sqrt{h}} = -\left(\frac{|\nabla h|^2}{8h^2} - \frac{\nabla^2 h}{4h}\right). \tag{11}$$

Taking the gradient of (11) one obtains the associated momentum equation

$$\frac{\partial \boldsymbol{u}}{\partial t} + (\boldsymbol{u}\cdot\nabla)\boldsymbol{u} + \nabla(h-1) + \nabla\left(\frac{|\nabla h|^2}{8h^2} - \frac{\nabla^2 h}{4h}\right) = \boldsymbol{F} \tag{12}$$

with the body force $\boldsymbol{F} = \nabla\varphi$. The third term is similar to the pressure gradient term in shallow water equation while the fourth term known as "quantum pressure" resembles the effect of surface tension. However, it needs to be borne in mind that the definition of $\boldsymbol{u}$ as the gradient of θ implies that the constraint

$$\nabla \times \boldsymbol{u} = 0 \tag{13}$$

holds in all regions where $\psi \neq 0$. This constraint can be circumvented pointwise at vortex locations, where $\psi = 0$. We will use the transformed equations (10), (12), and (13) as the governing equations from now on.

Finally, we may also note the exact equations for momentum and energy in flux form as

$$\frac{\partial (h\boldsymbol{u})}{\partial t} + \nabla\cdot\left\{h\boldsymbol{u}\boldsymbol{u} + \frac{\nabla h \nabla h}{4h} + \left(\frac{h^2}{2} - \frac{\nabla^2 h}{4}\right)\boldsymbol{I}\right\} = h\boldsymbol{F}, \tag{14}$$

$$\frac{\partial e}{\partial t} + \nabla\cdot\left\{e\boldsymbol{u} + \frac{h^2-1}{2}\boldsymbol{u} - \frac{\nabla^2 h}{4}\boldsymbol{u} + \frac{\nabla\cdot(h\boldsymbol{u})}{4h}\nabla h\right\} = h\boldsymbol{u}\cdot\boldsymbol{F}. \tag{15}$$

Here, the energy density $e = h|\boldsymbol{u}|^2/2 + |\nabla h|^2/(8h) + (h-1)^2/2$ is the integrand in (9).

C. Linear waves and ray tracing

The transformed equations will be studied with a regular perturbation expansion to second order in a suitable small-wave-amplitude parameter $a \ll 1$, i.e., there will be a (steady) $O(1)$ background flow $\{\boldsymbol{U}, H\}$, $O(a)$ linear waves $\{\boldsymbol{u}', h'\}$, and an $O(a^2)$ nonlinear mean-flow response to the waves. Eventually, we will assume that the waves form a slowly varying wavetrain, which allows averaging and the use of ray-tracing theory. Of course, one could also perform the perturbation expansion in terms of the wave function ψ in the original, untransformed NLS equation. For example, to $O(a)$ accuracy the asymptotic relations $\boldsymbol{u} \sim \boldsymbol{U} + \boldsymbol{u}'$ and $h \sim H + h'$ are consistent with $\psi \sim \Psi + \psi'$, say, provided that $\Psi = \sqrt{H}\exp(i\alpha)$ and $\psi'/\Psi = h'/2H + i\theta'$, where $\theta \sim \alpha + \theta'$ such that $\boldsymbol{U} = \nabla\alpha$ and $\boldsymbol{u}' = \nabla\theta'$ hold. However, it is much easier to study the nonlinear interplay between waves and vortices at $O(a^2)$ in the fluid variables, which is why we proceed in this manner.

Now, the full $O(a)$ equations for $\boldsymbol{u}'$ and h' are

$$\frac{\partial h'}{\partial t} + \nabla\cdot(H\boldsymbol{u}' + h'\boldsymbol{U}) = 0, \tag{16}$$

$$\frac{\partial \boldsymbol{u}'}{\partial t} + (\boldsymbol{U}\cdot\nabla)\boldsymbol{u}' + (\boldsymbol{u}'\cdot\nabla)\boldsymbol{U} + \nabla h' - \frac{1}{4}\nabla\left[\nabla^2\left(\frac{h'}{H}\right)\right] - \frac{1}{4}\nabla\left[\frac{\nabla H}{H}\cdot\nabla\left(\frac{h'}{H}\right)\right] = \boldsymbol{F}'. \tag{17}$$

Here, the irrotational linear force $\boldsymbol{F}'$ serves to represent wave emission and absorption. We will only solve these equations using the standard ray-tracing approximation, which is valid for a slowly varying wavetrain in a slowly varying background environment. Hence, we assume that the linear fields are given by the real part of the product between a slowly varying amplitude function and the

rapidly varying oscillatory function $\exp(i\Theta)$. Here, the rapidly varying wave phase Θ is not to be confused with the phase θ of the original wave function ψ in (7)!

The derivatives of the wave phase define the local wavenumber vector and frequency in the usual way and both must satisfy the standard dispersion relation based on a uniform background with constant density H and constant velocity $\boldsymbol{U}$

$$\boldsymbol{k} = \nabla\Theta, \quad \omega = -\Theta_t, \quad \omega = \hat{\omega} + \boldsymbol{U}\cdot\boldsymbol{k}, \quad \hat{\omega} = \sqrt{H\kappa^2 + \frac{\kappa^4}{4}}. \tag{18}$$

Here, $\boldsymbol{k}$ is the local wavenumber vector, ω is the absolute wave frequency, and the intrinsic frequency $\hat{\omega}$ is given in terms of $\kappa = |\boldsymbol{k}|$ by the dispersion relation in (18). From now on we restrict to two-dimensional dynamics such that $\boldsymbol{x} = (x, y)$ and $\boldsymbol{k} = (k, l)$. It then turns out that the dispersion relation in (18) is identical to that of the shallow water equations with surface tension.[20] Hence, for small wave numbers or long wavelengths, $\hat{\omega} \approx \sqrt{H}\kappa$ is a non-dispersive sound wave dispersion relation, whereas for higher wave numbers or short waves, $\hat{\omega} \approx \kappa^2/2$, which in quantum mechanics is the dispersion relation for free particles. This wave-number-dependent asymptotic behavior will be seen to give rise to the wave-number-dependence of the wave scattering angle due to vortices (see Sec. IV), which is different from the simpler classical theory in BM03.[17]

The standard ray-tracing equations for $\boldsymbol{x} = (x, y)$ and $\boldsymbol{k} = (k, l)$ as functions of time along group-velocity rays are given in terms of the absolute frequency function

$$\Omega(\boldsymbol{x}, \boldsymbol{k}, t) = \hat{\omega} + \boldsymbol{U}\cdot\boldsymbol{k} = \sqrt{H\kappa^2 + \kappa^4/4} + \boldsymbol{U}\cdot\boldsymbol{k} \tag{19}$$

by the standard Hamiltonian equations[20]

$$\frac{d\boldsymbol{x}}{dt} = +\frac{\partial\Omega}{\partial\boldsymbol{k}} \quad \text{and} \quad \frac{d\boldsymbol{k}}{dt} = -\frac{\partial\Omega}{\partial\boldsymbol{x}}, \tag{20}$$

where the time derivative along a ray is defined as

$$\frac{d}{dt} = \frac{\partial}{\partial t} + (\boldsymbol{c}_g\cdot\nabla) \tag{21}$$

acting on slowly varying functions of $(\boldsymbol{x}, t)$. The group velocity $\boldsymbol{c}_g$ is defined by

$$\boldsymbol{c}_g = (u_g, v_g) = \frac{d\boldsymbol{x}}{dt} = \hat{\boldsymbol{c}}_g + \boldsymbol{U} = \frac{2H + \kappa^2}{2\hat{\omega}}\boldsymbol{k} + \boldsymbol{U}. \tag{22}$$

For steady background fields, the ray-tracing equations imply that $d\omega/dt = 0$, i.e., the absolute frequency is constant along any group-velocity ray. In addition, if the background flow has azimuthal symmetry around the origin of the coordinate system, then there is another ray invariant, namely,

$$M = (\boldsymbol{r}\times\boldsymbol{k})_z = lx - ky. \tag{23}$$

This will be the case in Secs. III and VI below. The evolution of wave amplitude along a ray is governed by the conservation law for the wave action A at $O(a^2)$[21]

$$\frac{\partial(HA)}{\partial t} + \nabla\cdot(HA\boldsymbol{c}_g) = \frac{H}{\hat{\omega}}\overline{\boldsymbol{u}'\cdot\boldsymbol{F}'}, \tag{24}$$

where

$$A = \frac{E}{\hat{\omega}} \quad \text{and} \quad E = \frac{\overline{\boldsymbol{u}'^2}}{2} + \frac{\overline{h'^2}}{2H} + \frac{1}{8}\overline{\left|\nabla\left(\frac{h'}{H}\right)\right|^2} \tag{25}$$

is the wave energy per unit mass. The wave action is conserved in region where $\boldsymbol{F}' = 0$. For a steady unforced wavetrain, (24) reduces to

$$\nabla\cdot(HA\boldsymbol{c}_g) = 0. \tag{26}$$

A very important quantity in wave–mean interaction theory is the *pseudomomentum* vector[6]

$$\boldsymbol{p} = \boldsymbol{k}A = \boldsymbol{k}\frac{E}{\hat{\omega}} \tag{27}$$

per unit mass. For irrotational velocity fields and a slowly varying wavetrain,[6] we also have $\boldsymbol{p} = \overline{h'\boldsymbol{u}'}/H$. The pseudomomentum evolution can be shown to satisfy

$$\frac{\partial(H\boldsymbol{p})}{\partial t} + \boldsymbol{\nabla}\cdot(H\boldsymbol{p}\boldsymbol{c}_g) = HA\frac{d\boldsymbol{k}}{dt} + \overline{h'\boldsymbol{F}'} = -HA\frac{\partial\Omega}{\partial\boldsymbol{x}} + \overline{h'\boldsymbol{F}'}. \tag{28}$$

Unlike wave action, pseudomomentum can be created or destroyed without forcing or dissipation provided the background flow is inhomogeneous as measured by non-vanishing $\partial\Omega/\partial\boldsymbol{x}$. Physically, this corresponds to wave refraction caused by non-uniform H or $\boldsymbol{U}$: such refraction conserves wave action but not pseudomomentum.

III. REMOTE RECOIL WITH A SINGLE VORTEX

We follow BM03[17] and consider the refraction of a finite wavetrain passing a single vortex as depicted in Fig. 1. The $O(1)$ vortex is placed at the origin of the coordinate system and an $O(a)$ wavetrain of finite length $2L$ is passing it at a distance D, with $a \ll 1$ being the small wave amplitude. We assume that L and D have comparable size and that both are large compared to the healing length, which is unity, so the waves are passing the vortex *remotely*. The word *remotely* is used to emphasis that there is no physical overlap between the vortex and waves. To make the wavetrain length finite, we employ a suitably chosen linear force field $\boldsymbol{F}'$ that generates and absorbs the waves in the locations marked symbolically by the loudspeakers. There are two linked wave–vortex interaction effects in this situation, as discussed in detail in BM03.[17] First, the linear waves are refracted by the non-uniform background vortex flow. Second, the vortex experiences a *remote recoil*, namely, the vortex is expected to move slowly to the left due to advection by a nonlinear $O(a^2)$ mean flow induced by the finite wavetrain. Both effects combine to balance the global momentum budget.

The present superfluid situation differs in several important aspects from the classical fluid situation studied in BM03.[17] First, the strength of the vortex circulation cannot be chosen arbitrarily but is quantized.[22] Also, in BM03[17] the vortex had a finite size whereas here it is necessarily a point vortex. Second, here the dynamics of the linear waves depends on their wavelength whereas they

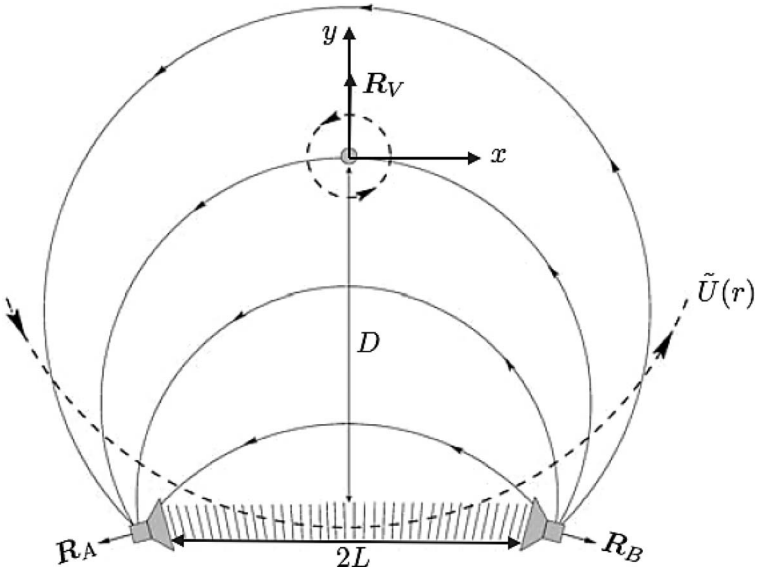

FIG. 1. A background vortex with circulation $\Gamma = 2\pi$ is passed at a distance $D \gg 1$ by a finite train of waves that are generated and absorbed in the locations marked by the loudspeakers. The waves are refracted by the $O(1)$ background vortex flow (dashed curves) and at the same time the vortex is exposed to an $O(a^2)$ large-scale return flow induced by the waves (solid curves). Specifically, the background velocity of the vortex pushes the waves toward decreasing y at the source and pulls them toward increasing y at the sink. To keep $y =$ constant along the rays, the phase lines have to tilt slightly as indicated. This leads to tilted recoil forces $\boldsymbol{R}_A$ and $\boldsymbol{R}_B$ at the loudspeakers and to a compensating remote recoil $\boldsymbol{R}_V$ at the vortex, see (29).

did not in BM03.[17] Third, in BM03[17] the vortex was held steady by a suitable holding force with nonzero curl and the integral over that holding force then provided the definition of the total recoil force $\boldsymbol{R}_V$, say, that is felt by the vortex. Here, this is not possible because only irrotational forces can arise in the equations. However, we are free to imagine a thought experiment in which the vortex is kept fixed by covering the vortex region with a small cylinder, say, and keeping the cylinder steady by some external holding force, thereby allowing the background flow to remain steady. We identify this holding force with (minus) the vortex recoil force $\boldsymbol{R}_V$, and we calculate it by integrating the momentum-flux equation (14) over a suitable control volume, which we take to be the large circle $r = D/2$. On this circle the flow is unforced and steady, the wave field is zero and the height field is close to its undisturbed value, which is unity. The momentum flux across the circle must then balance the holding force on the imagined cylinder. Specifically, we define the exact recoil force by

$$\boldsymbol{R}_V = -\oint_{r=D/2} \left\{ h\boldsymbol{u}\boldsymbol{u}\cdot\hat{\boldsymbol{n}} + \frac{\nabla h \nabla h}{4h}\cdot\hat{\boldsymbol{n}} - \left(\frac{(h-1)^2}{2} + \frac{h}{2}|\boldsymbol{u}|^2 + \frac{|\nabla h|^2}{8h} \right) \hat{\boldsymbol{n}} \right\} ds, \tag{29}$$

where ds and $\hat{\boldsymbol{n}}$ are the line element and outward normal on the large circle. This follows from (14) after eliminating a term containing $\nabla^2 h$ by using the steady unforced version of the Bernoulli theorem in (11) and discarding an irrelevant constant. As we shall see, this extra step greatly simplifies the perturbation expansion of the integral.

A. Background flow

The background vortex is a point vortex located at the coordinate origin and its associated velocity field is axisymmetric with circumferential velocity $\tilde{U}(r) = \Gamma/(2\pi r)$, where $\Gamma > 0$ is the circulation. Because $\boldsymbol{U}$ is the gradient of the phase of a single-valued wave function, the circulation of the vortex is necessarily quantized as $\Gamma = 2k\pi$, $k \in \mathbb{Z}$. Higher-order vortices are unstable and are likely to split into several first-order vortices. We will consider $\Gamma = 2\pi$ in detail but retain a general Γ in some of the expressions below. The background velocity field is

$$\boldsymbol{U} = (U, V) = \frac{\Gamma}{2\pi}\left(\frac{-y}{r^2}, \frac{+x}{r^2} \right) = \left(\frac{-y}{r^2}, \frac{+x}{r^2} \right). \tag{30}$$

The density field $H(r)$ goes to zero at the vortex location $r = 0$ and it asymptotes toward unity for large r. Specifically, in the far field $r \gg 1$ the density profile H is well approximated[23] from the Bernoulli equation by

$$H(r) \sim 1 - \frac{\tilde{U}^2(r)}{2} = 1 - \frac{1}{2r^2}. \tag{31}$$

For intermediate values of r, the shape of $H(r)$ is easily found numerically and, if wanted, a uniformly accurate expression for $H(r)$ is readily provided by the Padé approximation[24]

$$H(r) \approx \frac{\left(\frac{11}{16} + \frac{11}{96}r^2\right) r^2}{1 + \frac{2}{3}r^2 + \frac{11}{96}r^4}. \tag{32}$$

This is illustrated in Fig. 2. As in BM03,[17] a suitable small parameter measuring the remoteness of the wave–vortex interaction is

$$\epsilon = \frac{|\Gamma|}{2\pi D} = \frac{1}{D} \ll 1. \tag{33}$$

Now there are two small parameters, $a \ll 1$ for wave amplitude and $\epsilon \ll 1$ for vortex remoteness. It is necessary that $\epsilon \gg a$ such that the $O(\epsilon)$ background vortex can still be considered as a large background flow compared with the $O(a)$ linear waves. Notably, the far-field approximation (31) is correct to $O(\epsilon^2)$ on the circle $r = D/2$ in (29), and $\nabla H = O(\epsilon^3)$ there.

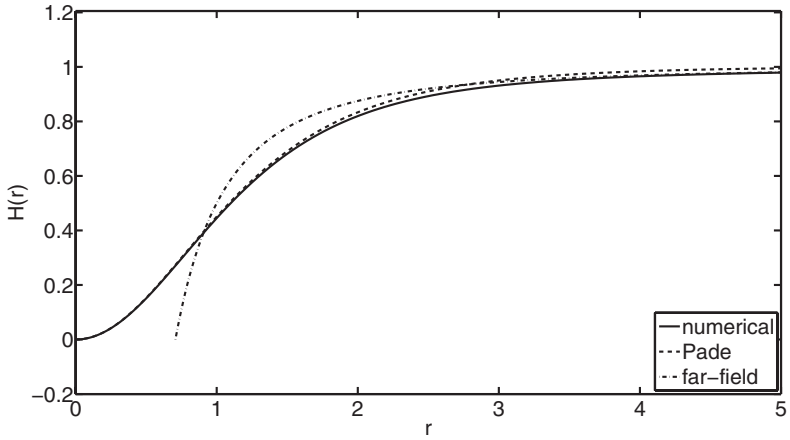

FIG. 2. Density field $H(r)$ of a single vortex. The solid line is the numerical solution, the dashed line is the Padé approximation in (32), and the dotted line is the far-field approximation in (31).

B. Linear waves

There is no general analytical method for solving the ray-tracing equations in the case of strong background flow gradients. However, as in BM03,[17] we will exploit the fact that these gradients are weak, of $O(\epsilon)$, along rays if the waves pass the vortex remotely. For example, this allows using the far-field approximation (31) to obtain the absolute frequency function up to $O(\epsilon^2)$ in the form

$$\omega = \hat{\omega} + \boldsymbol{U}\cdot\boldsymbol{k} \approx \sqrt{\kappa^2 + \frac{\kappa^4}{4}} + \boldsymbol{U}\cdot\boldsymbol{k} - \frac{1}{4}\frac{\tilde{U}^2}{\sqrt{1+\kappa^2/4}}\kappa. \tag{34}$$

Here, κ still needs to be computed along the ray, of course. The absolute group velocity function to the same approximation is

$$\boldsymbol{c}_g = \hat{\boldsymbol{c}}_g + \boldsymbol{U} \approx \frac{2+\kappa^2}{2\sqrt{\kappa^2+\kappa^4/4}}\boldsymbol{k} + \boldsymbol{U} - \frac{\tilde{U}^2}{4}\frac{\kappa^2}{\left(\kappa^2+\kappa^4/4\right)^{3/2}}\boldsymbol{k}. \tag{35}$$

We will assume that ω has the same value on all rays, which is consistent with a normal-mode approach. Now, the ray-tracing equations are still difficult to solve even truncated to $O(\epsilon^2)$. We will again follow BM03[17] and arrive at a useful wave solution by exploiting two important facts. First, it will turn out that knowing the wave field to $O(\epsilon^n)$ is enough to find the recoil force to $O(\epsilon^{n+1})$. For instance, ignoring the effect of the vortex for the wave structure is sufficient to compute the recoil force to $O(\epsilon)$, and using a first-order, $O(\epsilon)$ approximation for the waves is sufficient to compute the recoil force to $O(\epsilon^2)$. We will therefore be content if we can compute the wave field correctly only up to $O(\epsilon)$. At this level of approximation the far-field height field is simply $H \sim 1$ and the problem reduces to ray tracing through a weak irrotational incompressible mean flow. Here, we exploit the second fact, namely, we use the extension to dispersive waves[6,25] of the classical[26] result that non-dispersive wave rays through an irrotational incompressible flow are straight lines to $O(\epsilon)$. This result means that while $\boldsymbol{k}$ and hence the intrinsic group velocity $\hat{\boldsymbol{c}}_g$ are changed by refraction due to $\boldsymbol{U}$, the absolute group velocity $\boldsymbol{c}_g$ remains pointing in the same direction. Hence, if the wavemaker on the left is slightly tilted toward the vortex to make $v_g = 0$ at the source, $v_g = 0$ will continue to be zero along the ray, i.e., the ray is just $y = \text{const}$. As in BM03,[17] by combining this argument with the general constraint $\nabla \times \boldsymbol{k} = 0$ and evaluating (35) to $O(\epsilon)$, the wavenumber vector to $O(\epsilon)$ is easily computed to be

$$\boldsymbol{k} = (k_0, 0) - \frac{2\hat{\omega}_0}{2+k_0^2}\boldsymbol{U}, \quad \text{with} \quad \hat{\omega}_0 = \sqrt{k_0^2 + \frac{k_0^4}{4}}. \tag{36}$$

The corresponding absolute group velocity to $O(\epsilon)$ is

$$\boldsymbol{c}_g = \boldsymbol{U} + \frac{2H+\kappa^2}{2\hat{\omega}}\boldsymbol{k} = \left(\frac{2+k_0^2}{2\hat{\omega}_0}k_0 + \frac{8}{(2+k_0^2)(4+k_0^2)}U, 0\right) \tag{37}$$

and then the corresponding wave action density A follows from (26) with $H = 1$, which reduces to constant Au_g along rays away from the wave source or sink. The result to order $O(\epsilon)$ is

$$A(x, y) = A_s(y)\left(1 + \frac{\Gamma}{2\pi\gamma}\frac{y(L^2-x^2)}{(x^2+y^2)(L^2+y^2)}\right)\chi_{x\in[-L,L]}. \tag{38}$$

Here, χ is the characteristic function and $A_s(y)$ is the wave action profile across the wave train at the wave source or sink, which are equal by symmetry here. This wave action expression omits fine details such as the smooth matching to zero underneath the wave source and sink, but these fine details will not be relevant for the recoil computation. Finally, the parameter γ depends on k_0 via

$$\gamma = \frac{(2+k_0^2)^2(4+k_0^2)}{16\hat{\omega}_0}k_0 = \left(1+\frac{k_0^2}{2}\right)^2\sqrt{1+\frac{k_0^2}{4}}. \tag{39}$$

Note that $\gamma \sim k_0^5/8$ if k_0 is large and that $\gamma \sim 1$ if k_0 is small, which is the shallow-water limit of BM03.[17]

C. Mean-flow response

We define the mean flow by averaging over the rapidly varying wave phase in the usual way and denote the averaging process by an overbar, so, for example, $\overline{\boldsymbol{u}}$ is the mean velocity and $\overline{\boldsymbol{u}'} = 0$. The background flow is part of the mean flow and the leading-order nonlinear mean-flow response arises at $O(a^2)$. By the assumptions $1 \gg \epsilon \gg a$, it is convenient to introduce the following notations to distinguish the contributions at different powers of a and ϵ. A single subscript denotes the contribution at the corresponding power of a while a second subscript, if present, denotes the contribution at corresponding power of ϵ, thus

$$\overline{h} = H + \overline{h}_{20} + \overline{h}_{21} + \overline{h}_{22} + \cdots, \tag{40}$$

$$\overline{\boldsymbol{u}} = \boldsymbol{U} + \overline{\boldsymbol{u}}_{20} + \overline{\boldsymbol{u}}_{21} + \overline{\boldsymbol{u}}_{22} + \cdots. \tag{41}$$

This is also the relevant expansion of the *complete* flow field $(h, \boldsymbol{u})$ needed for the integral in (29), simply because the wave field is zero on $r = D/2$. It is now easy to verify by inspection that, as said before, to obtain the recoil force $\boldsymbol{R}_V$ from (29) at $O(a^2\epsilon)$ requires only the wave fields and the mean-flow response to zeroth order in ϵ. In fact, only $\overline{\boldsymbol{u}}_{20}$ is needed in the integral because $H \approx 1$ and therefore $\overline{h}_{20}$ does not contribute to (29) at $O(a^2)$. Two terms contribute at $O(a^2\epsilon)$, which can be combined using a vector identity to yield

$$\boldsymbol{R}_V = -\oint_{r=D/2}\overline{\boldsymbol{u}}_{20}\times(\boldsymbol{U}\times\hat{\boldsymbol{n}})\,ds = -\frac{\Gamma}{2\pi}\hat{\boldsymbol{z}}\times\int_0^{2\pi}\overline{\boldsymbol{u}}_{20}|_{r=\frac{D}{2}}\,d\theta. \tag{42}$$

To find $\overline{\boldsymbol{u}}_{20}$, we combine the constraint $\nabla\times\overline{\boldsymbol{u}}_{20} = 0$ with the average of the continuity equation (10) at $O(a^2)$, which for a steady mean flow is

$$\boldsymbol{U}\cdot\nabla\overline{h}_2 + \nabla\cdot(H\overline{\boldsymbol{u}}_2) = -\nabla\cdot(\overline{h'\boldsymbol{u}'}). \tag{43}$$

At zeroth order in ϵ, this implies

$$\nabla\cdot\overline{\boldsymbol{u}}_{20} = -\frac{1}{H}\nabla\cdot(\overline{h'\boldsymbol{u}'}) = -\nabla\cdot\boldsymbol{p}_{20} = -k_0\frac{\partial A}{\partial x}, \tag{44}$$

and now $\overline{\boldsymbol{u}}_{20}$ can be computed. Before doing this we note an important simplification of (42) that follows from the fact that the restriction of $\overline{\boldsymbol{u}}_{20}$ to the disk $r \le D/2$ is both irrotational and non-divergent, which means that the components of $\overline{\boldsymbol{u}}_{20}$ are harmonic functions on this restriction:

$\nabla^2\overline{\boldsymbol{u}}_{20} = 0$. Therefore, we can apply the mean-value property of harmonic functions to (42) and get the exact simplification

$$\boldsymbol{R}_V = -\Gamma\hat{\boldsymbol{z}} \times \overline{\boldsymbol{u}}_{20}(0,0). \tag{45}$$

This shows that the effective recoil force $\boldsymbol{R}_V$ at $O(a^2\epsilon)$ is given by the usual Magnus force expression[27] based on the value of the mean-flow response velocity at the vortex location. Now, $\overline{\boldsymbol{u}}_{20}$ is computed from $\nabla \times \overline{\boldsymbol{u}}_{20} = 0$ and (44) using the standard Green's function as

$$\overline{\boldsymbol{u}}_{20}(x,y) = \frac{1}{2\pi}\int\int \frac{(x-x',y-y')}{(x-x')^2+(y-y')^2}\left[-k_0\frac{\partial A}{\partial x}(x',y')\right]dx'dy'. \tag{46}$$

One can apply action density expression (38) to zeroth order in ϵ and approximate the slowly varying pre-factor in the integrand by its value at the source (sink). With $(x,y) = (0,0)$ this yields

$$\overline{\boldsymbol{u}}_{20}(0,0) \approx -\frac{k_0}{\pi}\frac{(L,0)}{L^2+D^2}\int_{-\infty}^{+\infty} A_s(y)dy. \tag{47}$$

The recoil force at $O(a^2\epsilon)$ is then given by

$$\boldsymbol{R}_V = \hat{\boldsymbol{y}}\frac{k_0\Gamma}{\pi}\frac{L}{L^2+D^2}\int_{-\infty}^{+\infty} A_s(y)dy. \tag{48}$$

This is precisely the same as the classical fluids result (4.24) in BM03.[17] The reason for this is that the wavenumber-dependent modulation of the action density A at $O(\epsilon)$ in (38) does not enter at this level of approximation. This will be different in Sec. IV, where wave scattering and recoil forces at $O(a^2\epsilon^2)$ are considered.

IV. SCATTERING WITH A SINGLE VORTEX

Again following BM03,[17] we let $L \to \infty$ to obtain the classical scattering problem, in which waves approach from and recede to spatial infinity. The evolution of $\boldsymbol{k}$ to $O(\epsilon)$ along the ray is governed by (36) implying that $l \to 0$ as $x \to \pm\infty$. Thus, $\boldsymbol{k}$ starts parallel to the x-axis at $x = -\infty$, goes toward the vortex as waves approach then away as they recede, before again becoming parallel to the x-axis at $x = +\infty$. As shown in (48), the magnitude of the vortex recoil force $\boldsymbol{R}_V$ at $O(a^2\epsilon)$ goes to zero as $1/L$ when $L \to \infty$, which implies that at $O(a^2\epsilon)$ $\boldsymbol{R}_V \to 0$ as $L \to \infty$. Clearly, to obtain a non-zero answer in the scattering limit $L \to \infty$ we have to go to the next order in ϵ, which is $O(a^2\epsilon^2)$. At this order, the outgoing and incoming wavenumber vectors differ by a finite amount proportional to the scattering angle of the wave. Once more, the $O(a^2\epsilon^2)$ recoil force can be computed using only the $O(a\epsilon)$ wave field and the $O(a^2\epsilon)$ mean-flow response. The wave solution to this accuracy was already given in (36)–(39), so we can now focus on the mean-flow response.

A. Mean-flow response and recoil force

We use (40) and (41) with $H \approx 1 - |\boldsymbol{U}|^2/2$ to evaluate $\boldsymbol{R}_V$ in (29) at $O(a^2\epsilon^2)$. Because $\nabla H = O(\epsilon^3)$, it turns out that (42) still holds with $\overline{\boldsymbol{u}}_{21}$ in place of $\overline{\boldsymbol{u}}_{20}$. Therefore, to calculate the recoil force, our main task is to find $\overline{\boldsymbol{u}}_{21}$. To do this, we combine $\nabla \times \overline{\boldsymbol{u}}_{21} = 0$ with the $O(a^2\epsilon)$ mean continuity equation

$$\nabla \cdot \bar{\boldsymbol{u}}_{21} = -\nabla \cdot \boldsymbol{p}_{21} - \boldsymbol{U} \cdot \nabla\overline{h}_{20}, \tag{49}$$

where $\boldsymbol{p}_{21}$ is the $O(a^2\epsilon)$ part of $\boldsymbol{p} = \boldsymbol{k}A$, which can be computed via (36) and (38) in the limit $L \to \infty$, which is $A = A_s(y)(1 - U/\gamma)$. We find $\overline{h}_{20}$ from the $O(a^2\epsilon^0)$ part of the Bernoulli theorem (11), which yields the modified Helmholtz equation (see Appendix A)

$$(\nabla^2 - 4)\overline{h}_{20} = \frac{2k_0^2}{\hat{\omega}_0}A = \frac{2k_0^2}{\hat{\omega}_0}A_s(y) \tag{50}$$

for the infinite wavetrain. In general, the Green's function of (50) that is zero at infinity is proportional to the modified Bessel function $K_0(2r)$, which decays as $\exp(-2r)$ at large distances $r \gg 1$ from the

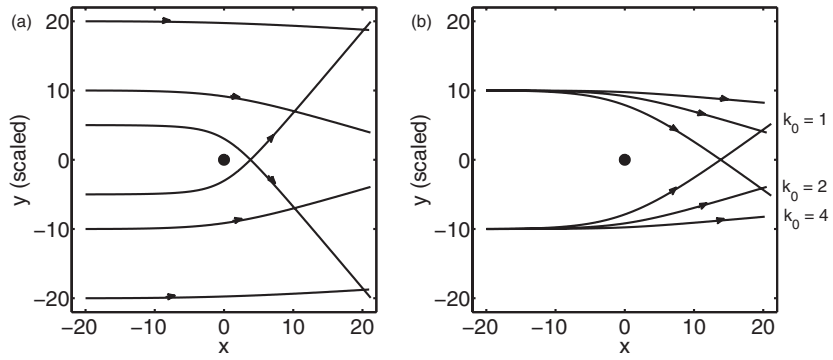

FIG. 3. (a) Numerical ray-tracing results for $k_0 = 1$ and various $y_0 = -D$. Rays are started from $|y_0| = \{5, 10, 20\}$ with the corresponding values for ϵ are $\{0.2, 0.1, 0.05\}$. The y-axis is rescaled by $y_0 + (y(t) - y_0)/0.05$ to show the scattering; (b) numerical ray-tracing results for $\epsilon = 0.1$ (or $|y_0| = 10$) and different k_0. The initial wavenumber k_0 are chosen to be $\{1, 2, 4\}$. The y-axis is rescaled by $y_0 + (y(t) - y_0)/0.02$ to show the scattering.

source. This makes obvious that $\overline{h}_{20}$ is nonzero only in the vicinity of the wavetrain. Moreover, by assumption the action density A is slowly varying compared to the healing length, which is unity in our scaled variables, and therefore the solution of (50) inside $r = D/2$ is well approximated by the slowly varying expression

$$\overline{h}_{20} = -\frac{k_0^2}{2\hat{\omega}_0} A = -\frac{k_0^2}{2\hat{\omega}_0} A_s(y) \quad \text{such that} \quad -\boldsymbol{U} \cdot \boldsymbol{\nabla} \overline{h}_{20} = \frac{k_0^2}{2\hat{\omega}_0} V \frac{dA_s}{dy}. \tag{51}$$

The accuracy of (51) is discussed in more detail in Appendix B. We can now repeat the earlier argument and conclude that the components of $\overline{\boldsymbol{u}}_{21}$ are harmonic on the restriction $r \le D/2$, and hence the recoil force at $O(a^2\epsilon^2)$ is again given by a Magnus formula, namely,

$$\boldsymbol{R}_V = -\Gamma \hat{\boldsymbol{z}} \times \overline{\boldsymbol{u}}_{21}(0, 0). \tag{52}$$

Inverting (49) with $\boldsymbol{\nabla} \times \overline{\boldsymbol{u}}_{21} = 0$ then provides the velocity at the vortex as

$$\begin{aligned} \overline{\boldsymbol{u}}_{21}(0, 0) &= \frac{1}{2\pi} \iint \frac{(-x, -y)}{x^2 + y^2} \left[\frac{k_0}{\gamma} \frac{\partial U}{\partial x} A_s(y) + \left(\frac{2\hat{\omega}_0}{2 + k_0^2} + \frac{k_0^2}{2\hat{\omega}_0} \right) V \frac{dA_s}{dy} \right] dx dy \\ &= \hat{\boldsymbol{x}} \frac{\Gamma k_0 \mathrm{sgn}(D)}{16\pi D^2} \left(\frac{1}{\gamma} + \frac{k_0}{\hat{\omega}_0} + \frac{(2 + k_0^2)(4 + k_0^2)}{4\gamma} \right) \int_{-\infty}^{+\infty} A_s(y) dy \end{aligned} \tag{53}$$

with γ given in (39). Consequently, the recoil force at $O(a^2\epsilon^2)$ for scattered waves is

$$\boldsymbol{R}_V = -\hat{\boldsymbol{y}} \frac{\Gamma^2 \mathrm{sgn}(D)}{16\pi D^2} \left(\frac{1}{\gamma} + \frac{k_0}{\hat{\omega}_0} + \frac{(2 + k_0^2)(4 + k_0^2)}{4\gamma} \right) k_0 \int_{-\infty}^{+\infty} A_s(y) dy. \tag{54}$$

The sign of the circulation does not matter for $\boldsymbol{R}_V$, but it does matter whether the waves pass to the right or the left of the vortex. We use $D > 0$ if the waves pass to the right, as exemplified by the lower rays in Fig. 3. Now, for small k_0 the bracket in (54) goes to 4, which recovers the classical shallow-water results in BM03.[17] Moreover, in this limit $k_0 A = k_0 E/\hat{\omega}_0 \to E$ and therefore at fixed wave energy density the recoil force goes to a nonzero limit as $k_0 \to 0$. Conversely, for large k_0 the bracket goes to $4/k_0$, which means the recoil force becomes proportional to the action density A in this limit. At fixed wave energy density $E = \hat{\omega}_0 A$, this means the recoil force tends to zero as $1/k_0^2$ as $k_0 \to \infty$.

B. Scattering angle and scale-selective refraction

From the recoil force at $O(a^2\epsilon^2)$, we can compute the global scattering angle θ_* of the waves. As described in BM03,[17] this is based on a global momentum budget argument, which gives an equality between $-\boldsymbol{R}_V$ and the total rate of change of pseudomomentum. The starting point is the

expression of $\boldsymbol{R}_V$ in (29). We will investigate the $O(a^2)$ terms in the limit $r \to \infty$ where r comes from the line element $ds = rd\theta$. It can be shown that (permitting $H = 1$ here)

$$\boldsymbol{R}_V = -\lim_{r\to\infty}\int_0^{2\pi}\left(\overline{\boldsymbol{u}'\boldsymbol{u}'} + \frac{1}{4}\overline{\nabla h'\nabla h'}\right)\cdot\hat{\boldsymbol{n}}rd\theta = -\lim_{r\to\infty}\int_0^{2\pi}\boldsymbol{p}\boldsymbol{c}_g\cdot\hat{\boldsymbol{n}}rd\theta. \tag{55}$$

This implies that the recoil force is equal to minus the difference between outgoing and incoming pseudomomentum fluxes, i.e., the recoil force is equal to minus the rate of change of pseudomomentum due to refraction by the vortex flow. The total wave action is conserved, hence the total rate of change of pseudomomentum is equal to the change in wavenumber vector times the total flux of conserved wave action along the wavetrain

$$\boldsymbol{R}_V = -(\boldsymbol{k}_- - \boldsymbol{k}_+)(\text{total wave action flux along wavetrain}), \tag{56}$$

where $\boldsymbol{k}_-$ and $\boldsymbol{k}_+$ are the incoming and outgoing wavenumber vectors, respectively. We use (56) to compute the scattering angle at $O(\epsilon^2)$ and since the wavenumber vector change is $O(\epsilon^2)$, the wave action flux need only to be computed at leading order $O(a^2\epsilon^0)$, which is

$$\text{total wave action flux along wavetrain} = \frac{2+k_0^2}{2\hat{\omega}_0}k_0\int_{-\infty}^{+\infty}A_s(y)dy. \tag{57}$$

Because of ray-invariance of absolute frequency, we have $|\boldsymbol{k}_-| = |\boldsymbol{k}_+|$ and therefore

$$\boldsymbol{k}_- - \boldsymbol{k}_+ = \theta_*\hat{\boldsymbol{z}}\times\boldsymbol{k}_- \tag{58}$$

for small θ_*. Now using (54), (56), and (57) and $\boldsymbol{k}_- = (k_0, 0)$ we obtain the nice expression

$$\theta_* = \pi\epsilon^2\text{sgn}(D)\left\{\frac{2}{(2+k_0^2)^3} + \frac{1}{(2+k_0^2)^2} + \frac{1}{2+k_0^2}\right\}. \tag{59}$$

For small k_0 this is consistent with the result $\theta_* = \pi\epsilon^2\text{sgn}(D)$ found in BM03.[17] For larger k_0 the scattering angle decrease sharply, as illustrated in Fig. 3. This should have notable consequences even in less idealized situations. For example, this suggests that if a broadband wave field were to pass the vortex, then one should find that the small-wavenumber components have been preferentially scattered into the lee of the vortex.

C. Numerical ray-tracing results

Numerical results are presented to test the theoretical predictions by integrating the ray-tracing equations (20) numerically with a standard Runge–Kutta scheme. This is done without any explicit expansion in $\epsilon \ll 1$ although the density field is approximated by (31) such that $\nabla H = (x, y)/r^4$. This yields

$$\begin{aligned}
\frac{dx}{dt} &= \frac{2H+\kappa^2}{2\hat{\omega}}k + U &&= \frac{2H+\kappa^2}{2\hat{\omega}}k - \frac{\Gamma}{2\pi}\frac{y}{r^2},\\
\frac{dy}{dt} &= \frac{2H+\kappa^2}{2\hat{\omega}}l + V &&= \frac{2H+\kappa^2}{2\hat{\omega}}l + \frac{\Gamma}{2\pi}\frac{x}{r^2},\\
\frac{dk}{dt} &= -\frac{\kappa^2}{2\hat{\omega}}\frac{\partial H}{\partial x} - U_x k - V_x l &&= -\frac{\kappa^2}{2\hat{\omega}}\frac{x}{r^4} - \frac{\Gamma}{2\pi}\frac{2xy}{r^4}k - \frac{\Gamma}{2\pi}\frac{y^2-x^2}{r^4}l,\\
\frac{dl}{dt} &= -\frac{\kappa^2}{2\hat{\omega}}\frac{\partial H}{\partial y} - U_y k - V_y l &&= -\frac{\kappa^2}{2\hat{\omega}}\frac{y}{r^4} - \frac{\Gamma}{2\pi}\frac{y^2-x^2}{r^4}k + \frac{\Gamma}{2\pi}\frac{2xy}{r^4}l.
\end{aligned} \tag{60}$$

The first column holds for any H and $\boldsymbol{U}$ while the second column uses H and $\boldsymbol{U}$ in (30) and (31). The initial conditions are $x(0) = -\infty$ (or a large enough negative number), $y(0) = -D$, $k(0) = k_0 > 0$, and $l(0) = 0$. Fig. 3(a) shows the results of a number of runs with varying $y(0) = -D$ and fixed $k_0 = 1$ with $\Gamma = 2\pi$. The figure is rescaled in the y-axis as described in the caption to highlight the scattering angle. The symmetry between waves passing to the left or to the right of the vortex can be observed. The scattering angle θ_r was computed for various values of ϵ and compared with the analytical predictions θ_* from (59). The results are collected in Table I. The last column clearly

TABLE I. Scattering results for $k_0 = 1$, $\Gamma = 2\pi$, and $y_0 = -D = -1/\epsilon$ is varied between runs. The predicted scattering angle θ_* is from (59), the angle θ_r comes from numerical integration of ray-tracing equations (60). The relative error Rel is defined by $(\theta_* - \theta_r)/\theta_r$.

D	ϵ	θ_*	θ_r	$(\theta_* - \theta_r)/\theta_r$	Rel/ϵ
5	0.20	0.065	0.046	0.42	2.1
10	0.10	0.016	0.013	0.21	2.1
20	0.05	0.0041	0.0037	0.11	2.1
50	0.02	0.00065	0.00063	0.043	2.1

shows that the relative error scales as ϵ, which suggests that the next term in the expansion of θ_* would be $\propto\epsilon^3$. Such a term would break the symmetry between waves passing to the left or right of the vortex that holds at $O(\epsilon^2)$.

Of course, what is special in superfluids is that the dispersion relation in (18) has different asymptotic behaviour for small and large wavenumber, so the important task is to vary k_0. Fig. 3(b) shows the results of a number of runs with varying k_0 while ϵ is kept constant. Numerical results of the scattering angle θ_r for various values of k_0 and comparison with analytical predictions θ_* from (59) are summarized in Table II. The last column suggests that the coefficient of the next term in the ϵ-expansion of θ_* might be proportional to $1/k_0$.

V. SCATTERING WITH MULTIPLE VORTICES

Our method also applies to scattering problem with multiple vortices. Similar to the single vortex case, we can cover each vortex region with a small cylinder and keep the cylinder steady by some external holding force. In this way, we can therefore assume n vortices are kept unmoved at location (x_i, y_i) with circulation Γ_i. As mentioned earlier, the vortex is quantized as $\Gamma_i = 2k\pi$, $k \in \mathbb{Z}$ and is stable for $k = \pm 1$ only. In order to have similar small parameter as ϵ in the single vortex case, we assume all vortices are far away from the wavetrain and define

$$1 \gg \epsilon_i = \frac{|\Gamma_i|}{2\pi(y_i + D)} = \frac{1}{y_i + D} \gg a, \tag{61}$$

where all ϵ_i are of the same size, which is comparable to ϵ.

A. Theoretical prediction

Previous results (36), (38), (49), and (50) are still valid, except that we need to change the velocity field $\boldsymbol{U}$ to

$$(U, V) = \boldsymbol{U} = \sum_{i=1}^{n} \boldsymbol{U}_i = \sum_{i=1}^{n} (U_i, V_i) = \sum_{i=1}^{n} \frac{\Gamma_i}{2\pi} \frac{(-(y - y_i), x - x_i)}{(x - x_i)^2 + (y - y_i)^2}, \tag{62}$$

TABLE II. Results for $\epsilon = 0.05$, $\Gamma = 2\pi$, and k_0 vary between runs. The predicted scattering angle θ_* is from (59), the angle θ_r comes from numerical integration of ray-tracing equations (60). The relative error Rel is defined via $(\theta_* - \theta_r)/\theta_r$.

k_0	θ_*	θ_r	$(\theta_* - \theta_r)/\theta_r$	Rel/ϵ
1	0.0041	0.0037	0.11	2.1
2	0.0016	0.0015	0.056	1.1
4	0.00046	0.00045	0.026	0.50
8	0.00012	0.00012	0.013	0.25

the superposition of the velocity fields induced by each vortex. Applying the inversion formula to (49) with the irrotational condition $\nabla \times \overline{\boldsymbol{u}}_{21} = 0$ gives

$$\overline{\boldsymbol{u}}_{21}(x_j, y_j) = \frac{1}{2\pi} \int\int \frac{(x_j - x, y_j - y)}{(x_j - x)^2 + (y_j - y)^2} \times \sum_{i=1}^{n} \left[\frac{k_0}{\gamma} \frac{\partial U_i}{\partial x} A_s(y) + \left(\frac{2\hat{\omega}_0}{2 + k_0^2} + \frac{k_0^2}{2\hat{\omega}_0} \right) V_i \frac{dA_s}{dy} \right] dxdy \tag{63}$$

with constants γ given in (39). Then following the Magnus force formula, total force felt by all vortices is

$$\boldsymbol{R}_V = -\sum_{j=1}^{n} \Gamma_j \hat{\boldsymbol{z}} \times \overline{\boldsymbol{u}}_{21}(x_j, y_j), \tag{64}$$

from which one can compute the scattering angle of the waves. To do this, we continue using the global momentum budget argument, which says the recoil force is equal to minus the rate of change of pseudomomentum. Then by (56)–(58) the total recoil force is

$$\boldsymbol{R}_V = -\theta_* \hat{\boldsymbol{z}} \times \boldsymbol{k}_- \frac{2 + k_0^2}{2\hat{\omega}_0} k_0 \int_{-\infty}^{+\infty} A_s(y') dy'. \tag{65}$$

Combine (63) and (64) we obtain the scattering angle of the wavetrain

$$\theta_* = \left[\frac{2}{(2 + k_0^2)^3} + \frac{1}{(2 + k_0^2)^2} + \frac{1}{2 + k_0^2} \right] \left\{ \sum_{i=1}^{n} \pi \epsilon_i^2 \operatorname{sgn}(y_i + D) + \sum_{i \neq j} \frac{2\Gamma_i \Gamma_j}{\pi^2} \int \frac{(y_i + D)(x' - x_i)(x' - x_j)}{[(x' - x_i)^2 + (D + y_i)^2][(x' - x_j)^2 + (D + y_j)^2]} dx' \right\}. \tag{66}$$

The integral in the formula can be explicitly calculated since the integrant is an integrable rational function. Detailed calculation can be found in Appendix C. Compared with the scattering angle for a single vortex in (59), the scattering angle in multiple vortices case contains two parts: one is the simple addition of the effects of every vortex with ϵ replaced by ϵ_i and D by $D + y_i$, while remains to be the distance between each vortex and the wavetrain; the other is the interactive effect between different vortices (the *i-j* term in the formula). Though a little weird, the interaction is not difficult to understand: in (49) the mean-flow response $\overline{\boldsymbol{u}}_{21}$ contains the contribution from all vortices manifested by the total velocity field $\boldsymbol{U}$. Therefore, in addition to feeling itself's mean-flow as in the single vortex case, each vortex is also in the responsive mean-flow induced by all other vortices.

B. Numerical results

As usual, we can numerically integrate the ray-tracing equations to double check our theoretical prediction in (66). Since the wavetrain is far away from all vortices, we use the far-field approximate background density H in (31) which is

$$H = 1 - \frac{|\boldsymbol{U}|^2}{2} \quad \text{hence} \quad \nabla H = -(\boldsymbol{U} \cdot \nabla)\boldsymbol{U} \tag{67}$$

by chain rule with $\boldsymbol{U}$ given in (62). Then the ray-tracing equations are given by the first equality in (60) with H and $\boldsymbol{U}$ following (62) and (67). To check the theoretical prediction θ_*, we focus on two horizontal (vertical) vortices of equal distance from the origin with opposite (same) circulation. Or more specifically, the vortex at $(-x_d, 0)$ or $(0, x_d)$ has circulation 2π in both cases while the one at $(x_d, 0)$ or $(0, -x_d)$ has circulation -2π for opposite circulation and 2π for same circulation case. The wavetrain starts from $x(0) = -\infty$ (or a large enough negative number), $y(0) = -D$ with initial wavevector $\boldsymbol{k}(0) = (k_0, 0)$. Fig. 4 shows the results of a number of runs with varying $y(0) = -D$ with all other parameters being kept constants. The figure magnifies the scattering angles by rescaling

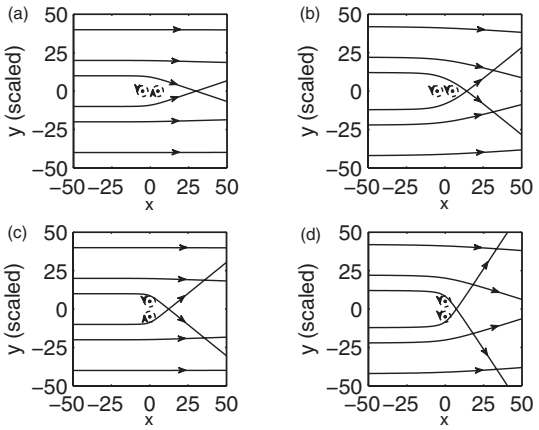

FIG. 4. Numerical ray-tracing results for (a) two vortices with opposite circulation $\pm 2\pi$ are at $(-5, 0)$ and $(5, 0)$. (b) Two vortices with positive circulation 2π are at $(-5, 0)$ and $(5, 0)$. (c) Two vortices with opposite circulation $\pm 2\pi$ are at $(0, 5)$ and $(0, -5)$. (d) Two vortices with positive circulation 2π are at $(0, 5)$ and $(0, -5)$. The initial wavenumber is $k_0 = 2$. Waves are started from $|y_0| = \{10, 20, 40\}$. The y-axis is rescaled by $y_0 + (y(t) - y_0)/0.02$ to highlight the scattering.

the y-axis as described in the caption. The symmetry between the left and right passing waves can be easily observed, which corresponds to being quadratic in terms of Γ in (66).

We can also calculate the relative error by comparing the numerical and analytic results. But unlike the single vortex case where the relative error is proportional to ϵ, there is no simple prediction of the next term in the asymptotic expansion because it also depends on the relative position of the wavetrain and all vortices.

VI. RAY COLLAPSE ONTO A VORTEX

If the waves get close to a vortex, then the interaction parameter ϵ is obviously not small anymore and the previous scattering analysis does not apply. The extreme case is where the wave ray actually spirals into the vortex and collapses to its centre in finite time. Clearly, ray collapse is a drastic change from the previous weak scattering and weak wave–vortex interaction situation. Its possibility was apparently first pointed out by Salant[18] in the context of two-dimensional acoustic waves outside a point vortex, with a later extension to three-dimensional acoustic waves by others.[28,29]

We will investigate the possibility for ray collapse in the nonlinear Schrödinger equation by using the NLS dispersion relation (70) below, and while taking the detailed density structure of the core into account. Using standard methods, we will find the criterion for ray collapse and investigate the structure of the collapsing rays. This is an extension of the earlier studies, which in their explicit results were restricted to acoustic waves and constant core density, so the underlying dispersion relation was $\omega = \kappa + \boldsymbol{U} \cdot \boldsymbol{k}$. As κ grows without bound during collapse, this inevitably fails to be a good approximation to the NLS dispersion relation (70), and this has significant consequences for the ray structure. We then discuss a necessary condition for ray tracing to remain valid even as the ray collapses onto a vortex and finally consider the inevitable wave amplitude growth during collapse.

A. Ray collapse condition

We assume the stationary axially symmetric vortex flow introduced in (30) with $\Gamma = 2\pi$

$$\boldsymbol{U} = U_\phi \hat{\boldsymbol{\phi}} = \frac{\Gamma}{2\pi}\frac{1}{r}\hat{\boldsymbol{\phi}} = \frac{1}{r}\hat{\boldsymbol{\phi}}, \quad H = H(r). \tag{68}$$

Since the ray can get arbitrarily close to the vortex, we use (32) or the numerical solution of the NLS equation to approximate the density field $H(r)$. Here, $\hat{\boldsymbol{r}}$ is the unit vector in the direction of $\boldsymbol{r} = (x, y)$ while $\hat{\boldsymbol{\phi}}$ is the unit azimuthal vector complying with the right-hand rule. By this choice,

one can decompose the wavenumber vector locally into

$$\boldsymbol{k} = \kappa_r \hat{\boldsymbol{r}} + \kappa_\phi \hat{\boldsymbol{\phi}}. \tag{69}$$

The Hamiltonian ray-tracing system (20) is integrable because it has two pairs of variables and also two independent invariants, which are here given by absolute frequency

$$\omega = \sqrt{H\kappa^2 + \kappa^4/4} + \boldsymbol{U}\cdot\boldsymbol{k} = \sqrt{H\kappa^2 + \kappa^4/4} + \kappa_\phi/r, \tag{70}$$

and the z-component of the aforementioned "angular momentum" invariant

$$M = (\boldsymbol{r}\times\boldsymbol{k})_z = lx - ky = r\kappa_\phi. \tag{71}$$

The previously studied acoustic case is included by setting $H = 1$ and ignoring the κ^4 term in (70). Substituting (69) and (71) into (70) yields

$$\omega = \sqrt{H\left(\kappa_r^2 + \left(\frac{M}{r}\right)^2\right) + \frac{1}{4}\left(\kappa_r^2 + \left(\frac{M}{r}\right)^2\right)^2} + \frac{M}{r^2} \tag{72}$$

or in terms of κ_r^2,

$$\kappa_r^2 = 2\sqrt{H^2 + \left(\omega - \frac{M}{r^2}\right)^2} - 2H - \frac{M^2}{r^2}. \tag{73}$$

Now, the standard argument for a collapse condition is based on the fact that r decreases along the ray only if the intrinsic group velocity points inward, which means $\kappa_r < 0$. Hence, a wavepacket will collapse onto the vortex if $\kappa_r < 0$ initially and if $|\kappa_r|$ remains bounded away from zero for all values of $r \geq 0$. Conversely, if κ_r goes through zero and changes sign, then the ray is simply scattered and escapes again to infinity. Therefore, the collapse condition is precisely the non-existence of a radius $r_* \geq 0$ where $\kappa_r = 0$. Assuming $\kappa_r = 0$ in (72) yields

$$\omega = \sqrt{H\frac{M^2}{r_*^2} + \frac{1}{4}\frac{M^4}{r_*^4}} + \frac{M}{r_*^2} \tag{74}$$

and hence the ray collapses precisely if this equation has no real positive solution for r_*. By construction the frequency ω is positive, but M may have either sign. As detailed in Appendix D it is easy to extract the necessary conditions $-2 \leq M \leq 0$ for collapse from (74). In other words, collapsing rays must propagate intrinsically against the spinning direction of the vortex, and the azimuthal progression of the wave phase, which is the physical interpretation of M, must be fairly modest and less than that of a mode-2 wave. The remaining condition on ω is found numerically and the full result is shown in Fig. 5, which depicts a convex-shaped parameter region of collapsing rays in the $M\omega$-plane. Fig. 6 illustrates the rays of several collapsing and non-collapsing wave rays, which cross-checks the theory in Fig. 5.

B. Comparison with acoustic rays

The structure of the collapsing rays in the present Schrödinger equation differs significantly from those in the previously studied acoustic equations. To begin with, as Fig. 6 illustrates, here rays can collapse onto the vortex by winding around the vortex in either a prograde or retrograde direction relative to the circulation sense of the vortex. This is in contrast with the acoustic case, in which the rays always wind in a prograde direction around the vortex. This occurs in the acoustic case because the azimuthal vortex velocity diverges as $r \to 0$ and therefore the prograde vortex flow must eventually dominate the intrinsic group velocity, which is bounded by the fixed acoustic wave speed. Not so in the Schrödinger case, where the intrinsic group velocity for large κ is proportional to κ, which by inspection of (70) and (72) obeys the scaling $\kappa \propto 1/r$ if $M \neq 0$. Therefore, the intrinsic retrograde group velocity (assuming $M < 0$) and the prograde vortex flow $U_\phi = 1/r$ are comparable in the present case, which allows one or the other to dominate during the collapse. Specifically, retrograde collapse occurs if $M < -1$ for the unit vortex with $U_\phi = 1/r$.

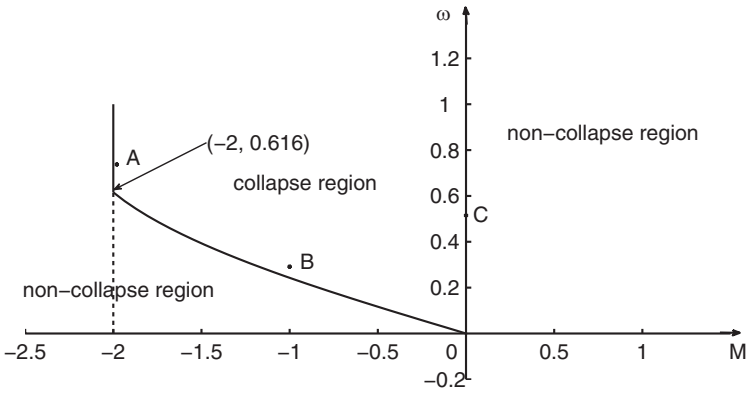

FIG. 5. Collapse region based on the dispersion relation (70). The boundary consists of the straight lines $M = 0$ and $M = -2$ and the connecting lower curve, which has been found numerically. The right boundary $M = 0$ is included in the collapse region, but not the others. For example, the lower-left point on the boundary is at $(-2, 0.616)$, which satisfies (74) with turning radius $r_* = 1.383$. Points A, B, and C correspond to the three panels in Fig. 6, respectively.

Another difference between the acoustic and the NLS case follows from the observation that if $M \neq 0$, then the intrinsic frequency $\hat{\omega} \propto 1/r^2$ and $k_\phi \propto 1/r$ in both cases, but $k_r \propto 1/r^2$ in the acoustic case while $k_r \propto 1/r$ in the NLS case. This means that in the acoustic case k_r dominates over k_ϕ and hence the wavenumber vector always turns precisely into the vortex as $r \to 0$, whereas in the NLS case k_r and k_ϕ are comparable and hence the wave crests come into the vortex with a finite angle of attack, which is a function of M. Finally, in both the acoustic and the NLS case the rays make an infinite number of revolutions around the vortex before reaching $r = 0$, but only in the acoustic case is the geometric length of the rays also infinite in any finite neighbourhood of the vortex. This is another repercussion of the asymptotically much faster intrinsic group velocity, and hence much more rapid collapse, in the NLS case compared to the acoustic case.

Of course, there are no true point vortices in any compressible fluid model such as the Navier-Stokes equations, for example, and hence there the actual, finite-size vortex structure must eventually be taken into account, which prohibits the strict collapse of acoustic rays onto a compressible vortex. The situation is different in the NLS equations, where true point vortices are natural and essential components of the dynamics. This warrants looking into the possible validity of ray tracing during the collapse in the NLS equations.

C. Validity of ray tracing during wave collapse

Ray tracing approximates linear wave theory under the assumption that the waves form a slowly varying wavetrain, so when ray tracing predicts a singular solution such as the formation of a wave

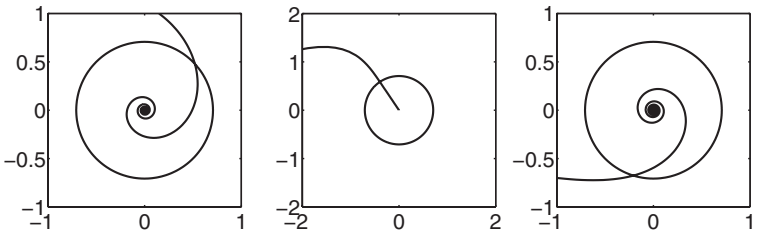

FIG. 6. A positive unit vortex is placed at $(0, 0)$ and the circle $r = 1/\sqrt{2}$ broadly marks the vortex core region, in which $H \leq 0.07$. Three different rays are shown, with initial conditions corresponding to the three points in Fig. 5. All rays are started at $(x, y) = (-5, 0)$. Left (point A): retrograde collapsing ray with $M = -1.998$, $\omega = 0.7373$, and $\boldsymbol{k} = (0.6574, 0.3996)$. Middle (point B): non-rotating ray with $M = -1.000$, $\omega = 0.2913$, and $\boldsymbol{k} = (0.2626, 0.2)$. Right (point C): prograde collapsing ray with $M = 0$, $\omega = 0.515$, and $\boldsymbol{k} = (0.5, 0)$.

caustic, where neighboring rays intersect, then this prediction may merely indicate that ray tracing has broken down, but not linear theory. On the other hand, ray tracing may remain valid all the way to the caustic, which then implies a singularity even in the full linear theory. This kind of situation is probably most familiar from the study of critical layers for dispersive waves, where ray tracing may or may not remain valid as the critical layer is approached, depending on the details of the dispersion relation.[6] Of course, this is a partial analogy at best. For example, experience with dispersive caustics at critical layers shows that the travel time to reach those caustics is infinite, whereas the travel time for collapsing waves to reach the vortex is decidedly finite.

In light of this difficult theoretical situation, we will simply consider here a necessary condition for the validity of ray tracing during wave collapse, which is that the slowly varying criterion $\kappa r \gg 1$ remains valid along the ray as $r \to 0$. This criterion measures whether the distance to the vortex appears "large" compared to the local wavelength; it is also easy to show that during one wave period the fractional change along group-velocity rays of both $\hat{\omega}$ and κ is proportional to $1/(\kappa r)^2$ as $r \to 0$.

First off, we notice the simple bound

$$r\kappa = r\sqrt{\kappa_r^2 + \kappa_\phi^2} \geq r|\kappa_\phi| = |M|, \tag{75}$$

but the equality holds only when $\kappa_r = 0$, i.e., when the ray does not collapse. For collapsing rays (75) is not very sharp and we can improve on it. Specifically, near the vortex $r \ll 1$ and hence by (73) and the approximation for $H(r)$ in (32) one can get

$$\kappa^2 = 2\sqrt{H^2 + \left(\omega - \frac{M}{r^2}\right)^2} - 2H = 2\omega - \frac{2M}{r^2} + O(r^2) \quad \Rightarrow \quad \kappa^2 r^2 \geq -2M. \tag{76}$$

This makes clear that ray tracing fails in the limiting case $M = 0$. As we know that for collapsing rays $-2 < M \leq 0$, these bounds suggest that ray tracing has the best chance of remaining valid for rays with M close to the limiting case $M = -2$, in which case $\kappa r \geq 2$. Of course, this is merely a finite-size bound, but ray tracing is often found to be surprisingly accurate in practice even if slowly varying criterion is not strongly satisfied. Our tentative conclusion is therefore that for values of M near $M = -2$, the collapse observed in ray tracing probably indicates a singular absorption of waves even in full linear theory.

This does raise further questions about collapsing waves that we unfortunately cannot answer here. For example, we ran some numerical experiments in which we followed neighbouring rays into the vortex in order to find out whether these rays will touch at some finite $r > 0$ and thereby form an external caustic, which would also invalidate ray tracing. Direct numerical integration of the ray-tracing equations shows the distance between neighbouring rays decays linearly in r and does not indicate any external caustic, but this is far from conclusive.

D. Asymptotic wave amplitude evolution during collapse

We can work out the wave amplitude predicted from ray tracing via the standard procedure of assuming a steady wavetrain and considering an infinitesimal ray tube formed of neighbouring rays such that the cross-sectional width of the tube is given by w, say. The (unforced) wave action conservation law (24) applied to the ray tube then yields

$$\nabla \cdot (HA\boldsymbol{c}_g) = 0 \quad \Rightarrow \quad HA|\boldsymbol{c}_g|w = \text{const} \tag{77}$$

along the tube. Now, in order to make progress, we assume that as $r \to 0$ the cross-sectional width w scales with r in the simplest self-similar way, which is $w \propto r$. (This appears almost inevitable given the azimuthal symmetry of the situation, where we could create a family of neighbouring collapsing rays by the simple device of rotating a single collapsing ray around the origin.) However, we also know that $|\boldsymbol{c}_g| \propto 1/r$, so the tendencies in these two terms cancel each other asymptotically in (77). This leads to the asymptotic structure of the action density as

$$HA = \text{const} \quad \Rightarrow \quad A \propto 1/H \propto 1/r^2. \tag{78}$$

Similarly, using $\kappa \propto 1/r$ and $\hat{\omega} \approx \kappa^2/2$, the pseudomomentum density $\boldsymbol{p} = \boldsymbol{k}A$ and the wave energy density $E = \hat{\omega}A$ are found to diverge even faster as

$$|\boldsymbol{p}| = \kappa A \propto 1/(Hr) \propto 1/r^3 \quad \text{and} \quad E \propto \kappa^2 A \propto 1/(Hr^2) \propto 1/r^4. \tag{79}$$

The validity of linear theory depends on the smallness of a suitable non-dimensional wave amplitude that measures the size of the ignored nonlinear terms against the size of the retained linear terms. The amplitude of nearly plane waves is typically given by the square root of $\overline{|\boldsymbol{u}'|^2}\kappa^2/\hat{\omega}^2$ or of the relative depth disturbance $\overline{h'^2}/H^2$. Both lead to the same result in the present case, which using (25) is

$$\text{amp}^2 \propto \overline{|\boldsymbol{u}'|^2}\frac{\kappa^2}{\hat{\omega}^2} \propto \frac{E}{\hat{\omega}}\frac{\kappa^2}{\hat{\omega}} \propto A \quad \Rightarrow \quad \text{amp} \propto \sqrt{A} \propto 1/\sqrt{H} \propto 1/r. \tag{80}$$

This divergence of the amplitude implies the breakdown of linear theory in some neighbourhood of the vortex location $r = 0$, which is quite consistent with the singular nature of the wave collapse.

VII. CONCLUDING REMARKS

Mutatis mutandis, our considerations of the remote recoil in the nonlinear Schrödinger equation has followed closely the previous computations in classical acoustic fluid dynamics that were described in BM03.[17] For the refraction of the linear waves by isolated vortices, the most significant difference was the wavenumber-dependence of the scattering process in the NLS system, which distinguished between the low-wavenumber regime, in which the classical acoustic results were recovered, and the high-wavenumber regime, in which the scattering behaviour was very different. Using the NLS as a simple mean-field model for the quantum mechanics of a Bose–Einstein condensate, the large-scale regime corresponds to collective particle motions while the small-scale regime corresponds to individual particle motions.

As far as the concomitant nonlinear back-reaction on the vortices is concerned, the main difference was that the use in BM03[17] of a vortical holding force could not be transferred to the NLS equation, where external forces are necessarily irrotational. Instead, we employed the standard method of computing the momentum budget for a large control volume $r = D/2$ surrounding the vortex, together with the observation that the $O(a^2)$ mean-flow response was harmonic on the restriction to this control volume, which allowed the use of the averaging theorem for harmonic functions. This construction again facilitated computing the wave scattering angle from a momentum budget, with results similar to the classical acoustic results in BM03.[17]

This contrasts with the phenomenon of collapsing rays onto a point vortex, which does not occur in classical acoustic fluids because there the vortex size is necessarily finite. Of course, the opposite restriction is true in the NLS system, in which all vortices are line vortices, or point vortices in the present two-dimensional situation. As shown in Sec. VI D, such a wave collapse must inevitably be accompanied by the divergence of the wave amplitude and therefore by a breakdown of linear theory near the vortex. It is fascinating to speculate about the nonlinear wave–vortex interactions that might take place in this case. For example, it is well understood that a divergent wave amplitude in classical fluid dynamics would lead to wave dissipation via nonlinear wave breaking and the concomitant generation of a dipolar mean-flow vorticity pattern at the edges of the breaking zone.[30] In this process, the pseudomomentum of the waves is converted into the hydrodynamical impulse of the freshly created dipolar vorticity field.[15] This kind of process is not exactly possible in the NLS equation because of its inherent restriction to point vortices, but it seems reasonable to expect that bundles of point vortices can be formed by breaking waves in the NLS equation, mimicking the analogous process in classical fluids and recovering the aforementioned conversion of wave pseudomomentum into vortical impulse. If this speculation is correct, then a collapsing wave ray would shower the original vortex with newly created vortex dipoles within a small wave breaking zone surrounding the original vortex! Investigating these strongly nonlinear aspects of the wave–vortex interactions in the NLS equation is of course outside the kind of theory we have available here.

Finally, we reiterate that real superfluid dynamics at finite temperature goes far beyond the NLS equation, even in the case of a dilute Bose–Einstein condensate. So from this point of view it is questionable whether the effects we have described here have observable counterparts in such superfluid systems. On the other hand, the NLS equation is a self-consistent and self-contained model paradigm for many physical systems, ranging from classical wave envelope dynamics to quantum mechanics, and therefore seeking to further our understanding of the intrinsic NLS dynamics is important in its own right.

ACKNOWLEDGMENTS

Financial support for Y.G. and O.B. under the U.S. National Science Foundation (NSF) Grant Nos. DMS-1009213, 1312159 and OCE-1024180 is gratefully acknowledged. We also thank the helpful comments from two anonymous referees for helping us improve the paper.

APPENDIX A: DEVIATION OF EQ. (50)

The Bernoulli equation (11) at $O(a^2)$ reads (let $\varphi = 0$)

$$(\nabla^2 - 4)\overline{h}_{20} = 2\overline{\boldsymbol{u}' \cdot \boldsymbol{u}'} + \overline{h'\nabla^2 h'} + \frac{\overline{|\nabla h'|^2}}{2}. \tag{A1}$$

We can write the linear fields explicitly by $\psi'/\Psi = C_1 e^{i\Theta} + C_2 e^{-i\Theta}$. Since we are only interested in the $O(a)$ waves, we can use the approximation $H = 1$. Therefore, the RHS of (A1) is

$$-2\kappa^2(C_1C_2 + C_1^*C_2^*) = 4\kappa^2\left(\hat{\omega} + \frac{\kappa^2}{2} + 1\right)|C_2|^2, \tag{A2}$$

and the $O(a^2)$ energy is

$$E = \frac{\overline{\boldsymbol{u}'^2}}{2} + \frac{\overline{h'^2}}{2H} + \frac{1}{8}\overline{\left|\nabla\left(\frac{h'}{H}\right)\right|^2} = 2\hat{\omega}^2\left(\hat{\omega} + \frac{\kappa^2}{2} + 1\right)|C_2|^2. \tag{A3}$$

With the definition of wave action $A = E/\hat{\omega}$, we can get Eq. (50), which is

$$(\nabla^2 - 4)\overline{h}_{20} = \frac{2\kappa^2}{\hat{\omega}^2}E = \frac{2\kappa^2}{\hat{\omega}}A \approx \frac{2\kappa_0^2}{\hat{\omega}_0}A_s(y). \tag{A4}$$

APPENDIX B: ACCURACY OF (51) IN DETERMINING $\overline{\boldsymbol{u}}_{21}$

The exact solution of (50) is

$$\overline{h}_{20} = -\frac{k_0^2}{2\hat{\omega}_0}\left\{\int_y^\infty e^{2(y-\xi)}A_s(\xi)d\xi + \int_{-\infty}^y e^{-2(y-\xi)}A_s(\xi)d\xi\right\}. \tag{B1}$$

The difference between this exact solution and the approximate one in (51) will decay as $-\exp(-2|y + D|)$ away from the wavetrain $y = -D$, which is a very small number inside $r \leq D/2$. Moreover, the difference integrates to 0 when calculating $\overline{\boldsymbol{u}}_{21}$.

APPENDIX C: INTEGRATION FOR MULTIPLE VORTICES

In (66), we need to calculate an integral of the form

$$\int \frac{(x' - x_i)(x' - x_j)}{[(x' - x_i)^2 + (D + y_i)^2]^2[(x' - x_j)^2 + (D + y_j)^2]}dx'. \tag{C1}$$

In order to simplify notation, let $a = x_i - x_j$, $b = D + y_i$, and $c = D + y_j$. Change variable using $x = x' - x_i$, (C1) reads

$$\int \frac{x(x+a)}{(x^2+b^2)^2[(x+a)^2+c^2]}dx. \tag{C2}$$

According to partial fraction decomposition, the integrant can be written as

$$\frac{\alpha x+\beta}{(x^2+b^2)^2} + \frac{Ax+B}{x^2+b^2} + \frac{-Ax+C}{(x+a)+c^2} \tag{C3}$$

while each part can be integrated explicitly, giving the results

$$\frac{\beta\pi}{2b^3}\mathrm{sgn}(b) + \frac{B\pi}{b}\mathrm{sgn}(b) + \frac{(C+aA)\pi}{c}\mathrm{sgn}(c), \tag{C4}$$

with the following constants:

$$\begin{aligned}
F &= a^4 + 2a^2b^2 + b^4 + 2a^2c^2 - 2b^2c^2 + c^4,\\
\alpha &= (a^3 + ab^2 + ac^2)/F, \quad \beta = (a^2b^2 - b^2c^2 + b^4)/F,\\
A &= (a^5 - 2a^3c^2 - 3ac^4 + 2a^3b^2 + 2ab^2c^2 + ab^4)/F^2,\\
B &= (-a^6 - a^4c^2 + a^2c^4 + c^6 - 2a^4b^2 - 4a^2b^2c^2 - 2c^4b^2 - a^2b^4 - c^2b^4)/F^2,\\
C &= (-a^6 + 5a^4c^2 + 5a^2c^4 - c^6 - 2a^4b^2 + 2b^2c^4 - a^2b^4 - b^4c^2)/F^2.
\end{aligned}$$

APPENDIX D: COLLAPSING CONDITION IN (M, ω) PLANE

We seek to find under what condition the equation

$$f(r) = \sqrt{H\frac{M^2}{r^2} + \frac{1}{4}\frac{M^4}{r^4}} + \frac{M}{r^2} = \omega \tag{D1}$$

has a finite positive solution $0 < r < \infty$ or not, the latter being the criterion for wave collapse. If $M > 0$, then

$$f(r) \to 0 \quad \text{as} \quad r \to \infty \quad \text{and} \quad f(r) \to \infty \quad \text{as} \quad r \to 0. \tag{D2}$$

Therefore, by the intermediate value theorem, there is at least one finite r that satisfies (D1), so $M \le 0$ is a necessary condition for collapse. Similarly, if $M < -2$, then

$$f(r) \to 0 \quad \text{as} \quad r \to \infty \quad \text{and} \quad f(r) > \frac{M^2+2M}{2r^2} \to \infty \quad \text{as} \quad r \to 0, \tag{D3}$$

since the numerator is bigger than zero for $M < -2$. Hence, the necessary condition for collapse is $-2 \le M \le 0$. If $M = 0$, then $f(r) \equiv 0$ and therefore (D1) does not have a solution for any $\omega > 0$, so these rays will collapse. For $-2 \le M < 0$, let $M = -\alpha\omega$ so that (D1) reads

$$\alpha\left(\sqrt{\frac{H}{r^2} + \frac{M^2}{4r^4}} - \frac{1}{r^2}\right) = 1. \tag{D4}$$

We call the function inside the brackets $g(r; M)$ and denote it maximum value over r by $G(M) = \max g(r; M)$, obtained at $r = r^*$. To have the equality in (D4), the minimum value of α can take is

$$\alpha^*(M) = \frac{1}{G(M)}. \tag{D5}$$

This means, if $\alpha < \alpha^*$, for any $r > 0$ the left-hand side in (D4) is always smaller than 1, i.e., there is no positive r satisfies (D4) or equivalently (D1). The wave packet will spiral in and finally collapse onto the vortex. For $\alpha > \alpha^*$, there is some $\tilde{r} > 0$ satisfies (D4) and the wave packet will travel toward the vortex till $r = \tilde{r}$ and then begin leaving the vortex region — it would not collapse onto the vortex. The maximum value G can be easily found numerically using the numerical density $H(r)$

and once known, using $M = -\alpha\omega$, one arrives at the collapse condition in the $M\omega$-plane shown in Fig. 5.

[1] J. Lighthill, *Waves in Fluids* (Cambridge University Press, 1978), p. 469.
[2] O. Bühler and T. E. Jacobson, "Wave-driven currents and vortex dynamics on barred beaches," J. Fluid Mech. **449**, 313 (2001).
[3] J. Vanneste and O. Bühler, "Streaming by leaky surface acoustic waves," Proc. R. Soc. A **467**, 1779–1800 (2011).
[4] R. Salmon, *Lectures on Geophysical Fluid Dynamics* (Oxford University Press, 1998), p. 362.
[5] G. K. Vallis, *Atmospheric and Oceanic Fluid Dynamics: Fundamentals and Large-Scale Circulation* (Cambridge University Press, Cambridge, UK, 2006), p. 745.
[6] O. Bühler, *Waves and Mean Flows* (Cambridge University Press, 2009).
[7] R. Donnelly, *Quantized Vortices in Helium II* (Cambridge University Press, 1991).
[8] *Quantized Vortex Dynamics and Superfluid Turbulence*, Lecture Notes in Physics Vol. 571, edited by C. Barenghi, R. Donnelly, and W. Vinen (Springer, 2001).
[9] C. J. Pethick and H. Smith, *Bose-Einstein Condensation in Dilute Gases* (Cambridge University Press, 2002).
[10] A. J. Leggett, *Quantum Liquids: Bose Condensation and Cooper Pairing in Condensed-Matter Systems* (Oxford University Press, Oxford, 2006), Vol. 34.
[11] D. J. Thouless, P. Ao, and Q. Niu, "Transverse force on a quantized vortex in a superfluid," Phys. Rev. Lett. **76**, 3758 (1996).
[12] M. Stone, "Iordanskii force and the gravitational Aharonov-Bohm effect for a moving vortex," Phys. Rev. B **61**, 11780 (2000).
[13] N. G. Berloff, "Quantum vortices, traveling coherent structures and superfluid turbulence," in *Contemporary Mathematics: Stationary and Time Dependent Gross-Pitaevskii Equations*, edited by A. Farina and J.-C. Saut (AMS, 2008), Vol. 473, p. 27.
[14] S. G. L. Smith, "Scattering of acoustic waves by a superfluid vortex," J. Phys. A **35**, 3597 (2002).
[15] O. Bühler, "Wave-vortex interactions in fluids and superfluids," Annu. Rev. Fluid Mech. **42**, 205 (2010).
[16] F. London, "The λ-phenomenon of liquid helium and the Bose-Einstein degeneracy," Nature (London) **141**, 643 (1938).
[17] O. Bühler and M. E. McIntyre, "Remote recoil: A new wave-mean interaction effect," J. Fluid Mech. **492**, 207 (2003).
[18] R. F. Salant, "Acoustic rays in two-dimensional rotating flow," J. Acoust. Soc. Am. **46**, 1153 (1969).
[19] E. Madelung, "Quanten theorie in hydrodynamischer form," Z. Phys. **40**, 322 (1927).
[20] G. B. Whitham, *Linear and Nonlinear Waves* (Wiley-Interscience, 1974).
[21] F. P. Bretherton and C. J. R. Garrett, "Wavetrains in inhomogeneous moving media," Proc. R. Soc. A **302**, 529 (1969).
[22] L. Onsager, "Statistical hydrodynamics," Nuovo Cimento Suppl. **6**, 279 (1949).
[23] J. C. Neu, "Vortices in complex scalar fields," Physica D **43**, 385 (1990).
[24] N. G. Berloff, "Padé approximations of solitary wave solution of the Gross-Pitaevskii equation," J. Phys. A **37**, 1617 (2004).
[25] K. B. Dysthe, "Refraction of gravity waves by weak current gradients," J. Fluid Mech. **442**, 157–159 (2001).
[26] L. D. Landau and E. M. Lifshitz, *Fluid Mechanics* (Pergamon, 1987).
[27] E. B. Sonin, "Magnus force in superfluids and superconductors," Phys. Rev. B **55**, 485 (1997).
[28] S. V. Nazarenko, "Absorption of sound by vortex filaments," Phys. Rev. Lett. **73**, 1793 (1994).
[29] S. V. Nazarenko, N. J. Zabusky, and T. Scheidegger, "Nonlinear sound-vortex interactions in an inviscid isentropic fluid: A two fluid model," Phys. Fluids **7**, 2407 (1995).
[30] O. Bühler, "On the vorticity transport due to dissipating or breaking waves in shallow-water flow," J. Fluid Mech. **407**, 235–263 (2000).